

# Accepted Manuscript

A full-angle Monte-Carlo scattering technique including cumulative and single-event Rutherford scattering in plasmas

Drew P. Higginson

PII: S0021-9991(17)30587-9  
DOI: <http://dx.doi.org/10.1016/j.jcp.2017.08.016>  
Reference: YJCPH 7518

To appear in: *Journal of Computational Physics*

Received date: 11 February 2017  
Revised date: 29 June 2017  
Accepted date: 7 August 2017

Please cite this article in press as: D.P. Higginson, A full-angle Monte-Carlo scattering technique including cumulative and single-event Rutherford scattering in plasmas, *J. Comput. Phys.* (2017), <http://dx.doi.org/10.1016/j.jcp.2017.08.016>

This is a PDF file of an unedited manuscript that has been accepted for publication. As a service to our customers we are providing this early version of the manuscript. The manuscript will undergo copyediting, typesetting, and review of the resulting proof before it is published in its final form. Please note that during the production process errors may be discovered which could affect the content, and all legal disclaimers that apply to the journal pertain.



## Highlights

- A self-consistent full-angle Rutherford scattering method for plasmas is defined.
- The method discretely transitions from cumulative to single-event scattering.
- Verification is performed using finely resolved discrete Monte-Carlo scattering.
- Regimes where this method is important are discussed.
- Test problems: interpenetrating plasma flows and keV-temperature equilibration.

# A full-angle Monte-Carlo scattering technique including cumulative and single-event Rutherford scattering in plasmas

Drew P. Higginson

*Lawrence Livermore National Laboratory, Livermore, California 94551, USA*

## Abstract

We describe and justify a full-angle scattering (FAS) method to faithfully reproduce the accumulated differential angular Rutherford scattering probability distribution function (pdf) of particles in a plasma. The FAS method splits the scattering events into two regions. At small angles it is described by cumulative scattering events resulting, via the central limit theorem, in a Gaussian-like pdf; at larger angles it is described by single-event scatters and retains a pdf that follows the form of the Rutherford differential cross-section. The FAS method is verified using discrete Monte-Carlo scattering simulations run at small timesteps to include each individual scattering event. We identify the FAS regime of interest as where the ratio of temporal/spatial scale-of-interest to slowing-down time/length is from  $10^{-3}$  to 0.3–0.7; the upper limit corresponds to Coulomb logarithm of 20–2, respectively. Two test problems, high-velocity interpenetrating plasma flows and keV-temperature ion equilibration, are used to highlight systems where including FAS is important to capture relevant physics.

## Contents

<b>1</b>	<b>Introduction</b>	<b>1</b>
<b>2</b>	<b>Previous Work for Cumulative Only Scattering</b>	<b>3</b>
2.1	Details of Nanbu's Model . . . . .	3
2.2	Large-Angle Legendre Polynomial Decomposition . . . . .	5
<b>3</b>	<b>Method for Full-Angle Scattering</b>	<b>5</b>
3.1	Derivation of the New Probability Distribution Function . . . . .	5
3.2	Numerical Implementation . . . . .	6
3.3	Summary of New Full-Angle Scattering Method . . . . .	8
3.4	Benchmarking Against Discrete Monte-Carlo Scattering Results . . . . .	9
3.5	Regimes of Interest for Full-Angle Scattering . . . . .	13
<b>4</b>	<b>Physical Systems of Interest</b>	<b>14</b>
4.1	Interpenetrating Plasma Flows . . . . .	14
4.2	Temperature Equilibration . . . . .	15
<b>5</b>	<b>Summary</b>	<b>17</b>

## 1. Introduction

Collisional binary interactions (i.e. Coulomb collisions) in a plasma range from very small to very large impact parameters,  $b$ ; these impacts result in large and small deviations in the polar scattering angle,  $\theta$ , respectively. The

*Email address:* [higginson2@llnl.gov](mailto:higginson2@llnl.gov) (Drew P. Higginson)

shape of Coulomb potential means that the interaction cross-section is strongly dependent on the impact parameter ( $\propto b^2$ ); this means scattering at smaller angles is much more likely and gives a strong inverse dependence ( $d\sigma/d\Omega \propto \sin^{-4}(\theta/2)$ ) to the differential cross-section, known as Rutherford scattering. In general, one would like to know the accumulated differential cross-section (i.e. the effective differential cross-section after multiple Rutherford scattering events) for a given path-length. One method to do this involves using the strong dependence on angle to suggest a separation of scales into cumulative (i.e. “small-angle”) and single-event (i.e. “large-angle”) scattering[1, 2, 3, 4]. When the number of collisions per particle,  $N$ , is high ( $N \gg 1$ ), scattering can be described by a diffusive or random-walk process. These scattered particles tend toward a Gaussian-like probability distribution function (pdf) due to the central-limit-theorem, and the width of this function increases with the number of collisions. On the other hand, when the number of collisions is small ( $N \ll 1$ ) a single collision is responsible for the deflection of a particle to a given angle. In contrast to the cumulative behavior, where the width of the pdf increases, for single-events the height of the pdf increases linearly with the number of collisions and retains the same shape (i.e.  $\propto \sin^{-4}(\theta/2)$ ). Concerning nomenclature in this study, we use will cumulative scattering instead of “small-angle,” as used by some, because this portion of the pdf can extend to all angles and is therefore not necessarily small. Also, another definition of small-angle is  $\sin x \simeq x$  (e.g. in the Rutherford cross-section); an approximation we do not use in this work. We use the term single-event scattering instead of “large-angle” for the same reason.

There are a variety of ways to incorporate Monte-Carlo scattering techniques into numerical simulations (see overviews in Refs. [5, 6, 7]) that accurately capture scattering. The most straightforward method is to use a timestep, or equivalently, path-length, that is small enough to resolve each individual collision, a method that we call discrete Monte-Carlo scattering (DMCS). In this method, the cumulative and single-event regions of the scattered pdf arise naturally as they would in a physical setting. In some situations, such as in a plasma where the Coulomb logarithm,  $\ln \Lambda$ , is small, this method may be feasible. However, often (e.g moderate  $\ln \Lambda$ ) resolving each individual collision is computationally impossible. To address this in Monte-Carlo codes modeling solid matter, the “condensed history” method[5] is often used. This method propagates particles for a finite, often predetermined, path-length and then scatters them using angular deflections either 1) as calculated using a Legendre decomposition[8] (e.g. ETRAN[9], ITS[10], MCNP[11]) or 2) using a mixture of cumulative collisions and discrete “catastrophic” collisions (e.g. EGS4[12]). In such codes, each particle trajectory can be modeled independently of the others and thus the path-length for each timestep can be chosen for accuracy; this is a major contrast to simulations modeling plasmas where each particle interacts with temporally evolving electric and magnetic fields meaning that all particles must evolve at the same timestep.

In contrast to the work in solid materials, most scattering models for plasmas, such as those included in particle-in-cell (PIC) codes[13, 14] and Vlasov-Fokker-Planck (VFP) codes[15], simply ignore single-event scatters and include only cumulative scattering. For many situations this is logical as these cumulative collisions are responsible for the majority of the momentum exchange. Also, neglecting single-event scattering will not decrease the “collisionality” of the plasma (i.e. energy/momentum exchange, temperature equilibrium), because the extra collisionality from these events is incorporated into the width of the cumulative scattering distribution. However, the results will not necessarily be a complete description of the full pdf as a function of angle (see Sec. 3.5 for more details). In fact, such situations where the tails or extrema of the pdf are important (e.g. neutron production, resonant phenomena) and when they evolve on scales faster than the collision rate, the inclusion of single-events can be important. For instance, in the case of low density interpenetrating flows with modest collisionality[16], including the single-event collisions is necessary to capture the dynamics of neutron generation due to the strong dependence of the nuclear cross-section on velocity (see Sec. 4).

Previous work has been done on inclusion of large-angle scattering in plasmas; for instance, a good overview of the work can be found in the paper by Turrell, Sherlock and Rose[17]. This paper describes an excellent method for introducing large-angle events into a code, however it is not completely self-contained in the sense that the transition angle between cumulative and single angle events is chosen somewhat arbitrarily. To our knowledge, there is not yet a fully self-consistent method of combining the cumulative and single-scattering events for Rutherford collisions in a plasma. In this Article, we define a method that creates a continuous distribution function that seamlessly transitions from cumulative to single-event scattering that we call full-angle scattering (FAS). Similar to standard cumulative-only algorithms (e.g. [14]), this method enforces the preservation of the correct angular variance (i.e. “angular width” or first-moment) at all times. This constraint, coupled with the need to preserve the particle number (i.e. zeroth-moment) and a continuous distribution creates a defined pdf. We use this pdf to create a inverted cumulative distribution function

that can be used for scattering particles in PIC or other Monte-Carlo type codes.

In addition to this work, a companion paper by Cohen *et al.* [18] describes a somewhat similar scattering algorithm specifically focused on the scattering of electrons in air. The method by Cohen *et al.* follows a treatment in Jackson's *Classical Electrodynamics* textbook, which makes the small-angle approximation of  $\theta \simeq \sin \theta$ . For this reason, we expect that the method presently described is more general and, thus, preferable to a broader range of plasma physics problems. Of particular note is their use of a lookup table approach to solving the set of equations (to be described in this paper) in contrast to the looped approach used here.

## 2. Previous Work for Cumulative Only Scattering

### 2.1. Details of Nanbu's Model

In order to understand the work that we have done in this Article, it is informative to review the previous work that has been done using (small-angle) cumulative only scattering. Perhaps the most commonly used collision method in particle-in-cell (PIC) simulations is the Nanbu collision operator[14, 19]. Interestingly, many of the insights from this paper were derived semi-empirically by running a Monte-Carlo collisional routine and evaluating the outputs. However, we note that other authors have come up with very similar[20], if not identical formulas that come from a more rigorous treatment of scattering via expansion into Legendre polynomials[8, 21]. The Monte-Carlo routine used by Nanbu scattered particles via the Rutherford scattering formula, where particles were given a polar deflection angle,  $\theta$ , randomly with a random number  $\mathcal{U}$  uniformly distributed between 0 and 1, based on the formula

$$\theta = 2 \tan^{-1}(\theta_{\min} / \sqrt{4\mathcal{U}}), \quad (1)$$

$$\text{where } \theta_{\min} = 2 \tan^{-1}\left(\frac{b_{\perp}}{b_{\max}}\right), \quad (2)$$

$$b_{\perp} = \frac{|q_i q_j|}{4\pi\epsilon_0 m_{ij} v_{ij}^2}, \quad (3)$$

$q$  is the charge of each particle,  $\epsilon_0$  is the vacuum permittivity,  $m_{ij}$  is the reduced mass and  $v_{ij} = |v_i - v_j|$  is the relative velocity between the two particles. The particles are then distributed uniformly into the azimuthal angle,  $\varphi$ . This method is equivalent to evaluating the Rutherford cross-section with the bounds from  $\theta_{\min}$  to  $\pi$ , where  $d\sigma_R/d\Omega = 0$  below  $\theta_{\min}$ :

$$\frac{d\sigma_R}{d\Omega} = \frac{b_{\perp}^2}{4 \sin^4 \frac{\theta}{2}} \quad \text{for } \theta > \theta_{\min} \quad (4)$$

From this Monte-Carlo technique, Nanbu noticed two features: 1) the angular distribution function ( $dn/d\Omega$ ) has a nearly logarithmic dependence with  $\cos \theta$  (i.e.  $\propto \exp[-2 \sin^2 \theta/2] \simeq \exp[-\theta^2/2]$ ) and, 2) the angular variance,  $\bar{\mu}_f$ , defined for the function  $f(\theta)$  as

$$\bar{\mu}_f \equiv \left\langle \sin^2 \frac{\theta}{2} \right\rangle_f = \frac{2\pi \int \sin \theta \sin^2 \frac{\theta}{2} f(\theta) d\theta}{2\pi \int \sin \theta f(\theta) d\theta}, \quad (5)$$

increases in a way that is nearly linearly with path-length. In this paper we use the convention

$$\mu = \sin^2(\theta/2) = \frac{1}{2}(1 - \cos \theta) \quad (6)$$

for simplicity. Nanbu used the first observation to create a normalized pdf,  $n(\theta)$ ,

$$n(\theta) = \frac{\alpha_n A}{2\pi} \exp\left(-2A \sin^2 \frac{\theta}{2}\right), \quad (7)$$

where here we have rearranged some terms from Nanbu's original formula (eq. 12 in [14]) to show clearly that the formula is very similar to a Gaussian. This is pdf is normalized using  $\alpha_n = 1/(1 - e^{-2A})$  and the angular variance of this function is  $\bar{\mu}_n = \frac{1}{2} \left[1 - \coth A + \frac{1}{A}\right]$ . We note that for this pdf, as for all pdfs in this paper, is defined as a function

of  $d\Omega$ , meaning that  $2\pi \int n(\theta) \sin \theta d\theta = 1$ . Nanbu's second observation was that the total angular variance of the Monte-Carlo Rutherford scattering,  $\bar{\mu}_{\text{total}}$ , increases via the formula,

$$\bar{\mu}_{\text{total}} = \frac{1}{2}(1 - e^{-s}). \quad (8)$$

In this equation,  $s = 2\bar{\mu}_R N$  is the normalized path-length, where  $\bar{\mu}_R$  is the angular variance of the Rutherford scattering function,  $N = \sigma_R v_{ij} n_j dt$  is the number of Rutherford scattering events, and  $\sigma_R$  is the total cross-section for Rutherford scattering. We note that in the specific case using the Rutherford cross-section in (4), that  $\sigma_R = \pi b_{\text{max}}^2$  and

$$\bar{\mu}_R = 2 \frac{b_{\perp}^2}{b_{\text{max}}^2} \ln \sqrt{\frac{b_{\text{max}}^2 + b_{\perp}^2}{b_{\perp}^2}}. \quad (9)$$

However this can vary slightly depending on the way that the differential cross-section varies at small angles.<sup>1</sup> Taking the limit of small path-length, we see clearly from (8) that for small values of  $s$ ,  $\langle \theta^2 \rangle_{\text{total}} \approx N \langle \theta^2 \rangle_R$  (i.e.  $\bar{\mu}_{\text{total}} \approx N\bar{\mu}_R$ ). Thus the angular variance grows linearly at small  $s$ . At the other extreme, as the normalized path-length gets very large ( $s \gg 1$ ) the value of  $\bar{\mu}_{\text{total}}$  becomes 1/2 meaning that the scattering is isotropic. Often, it is more useful to write  $s$  in terms of the Coulomb logarithm, which we define as

$$\ln \Lambda \equiv \frac{\sigma_R \bar{\mu}_R}{2\pi b_{\perp}^2}, \quad (10)$$

$$\text{thus, } s = 4\pi b_{\perp}^2 v_{ij} n_j dt \ln \Lambda. \quad (11)$$

In our specific case, we note that  $\ln \Lambda = \ln \sqrt{(b_{\text{max}}^2 + b_{\perp}^2)/b_{\perp}^2} \simeq \ln(b_{\text{max}}/b_{\perp})$ , where  $b_{\text{max}}$  is often chosen as the Debye length. Thus, the final step in Nanbu's method is to set the angular variance of  $n(\theta)$  to the known angular variance for a given value of  $s$  (i.e.  $\bar{\mu}_{\text{total}} = \bar{\mu}_n$ ). This gives the equation,

$$\frac{1}{2}(1 - e^{-s}) = \frac{1}{2} \left[ 1 - \coth A + \frac{1}{A} \right], \quad (12)$$

which can be solved numerically to give the inverse width  $A$  as a function of  $s$ . The pdf,  $n(\theta)$ , can be normalized and inverted to give the following scattering angle as a function of the uniformly distributed random number  $\mathcal{U}$ .

$$\cos \theta = 1 + \frac{1}{A} \ln \left[ 1 - \mathcal{U} (1 - e^{-2A}) \right] \quad (13)$$

We note that this equation is different, yet equivalent to the one used in Nanbu's paper (i.e. eq. 17 in [14];  $\cos \theta = \frac{1}{A} \ln [e^{-A} + 2\mathcal{U}' \sinh A]$ ) and can be recovered by using the transformation  $\mathcal{U} = 1 - \mathcal{U}'$ . However, we find this newer equation to be more useful than the original because it is numerically stable at both large or small values of  $A$ , while Nanbu's method has difficulties at both high and low values of  $A$  due to exponential overflow of  $\sinh A$ .

Nanbu's method captures both the total number (zeroth-moment) and the angular variance (first-moment). This method reproduces analytical temperature equilibration [3, 22] curves, showing the physical importance of correctly capturing the angular variance. However, we note the Nanbu's method is only strictly valid when the moment change in the particles is low. This is obvious, as we notice that Nanbu's method assumes that  $b_{\perp}$  and thus the relative velocity,  $v_{ij}$ , are constant. Later work by Dimits[23] also showed this limitation by showing that Nanbu's distribution is an approximation to the Coulomb-Lorentz kernel,

$$f_{CL}(\theta) = \frac{1}{2\pi} \sum_{l=0}^{\infty} \left( l + \frac{1}{2} \right) P_l(\cos \theta) \exp[-l(l+1)s], \quad (14)$$

where  $P_n$  is the Legendre Polynomial. This formula is valid when there is no energy exchange between scattering particles and when the scattering events considered are only cumulative (i.e. no large-angle single-event collisions).

<sup>1</sup>There are different scattering cross-sections that one might use instead of (4), for instance,  $\frac{d\sigma_R}{d\Omega} = b_{\perp}^2/[4 \sin^2(\theta/2) + 4 \sin^2(\theta_{\text{min}}/2)]^2$ . This will slightly change the value of the angular variance and thus the Coulomb logarithm. We have written most of these equations in a form so that the choice of exact cross-section is not fixed and can be chosen by the reader as desired.

This Coulomb-Lorentz kernel is the correct method to evaluate diffusion of velocity phasespace over a sphere. It is often called pitch-angle scattering and is a method used frequently in VFP simulations. Our new method will not overcome this limitation of small momentum exchange and thus we expect that it will be valid over the same regions as Nanbu's original operator, which requires the collision frequency to be resolved by a factor of around 100 for accurate solutions with similar mass-ratios[24, 23].

## 2.2. Large-Angle Legendre Polynomial Decomposition

We note now that another possible method to extend the collision operator into larger angles would be to use a Legendre polynomial expansion of the Rutherford cross-section without making the small-angle approximation. This method is described in [20] and originates from work by Goudsmit and Saunderson[8] and by Lewis[21]. This method uses the pdf,  $f_{GSL}(\theta)$ :

$$f_{GSL}(\theta) = \frac{1}{2\pi} \sum_{l=0}^{\infty} \left(l + \frac{1}{2}\right) \exp(-s/\tilde{s}_l) P_l(\cos \theta), \quad (15)$$

$$\text{where } \tilde{s}_l^{-1} = (2\pi/\sigma_R) \int_{-1}^1 [1 - P_n(\cos \theta)] (d\sigma_R/d\Omega) d(\cos \theta). \quad (16)$$

We attempted this approach, however it was not deemed feasible considering the numerical expense of calculating all of the polynomials in the expansion. In fact, using more than 1000 polynomials we were not able to get good convergence of the pdf, and the polynomial was not considered numerically accurate (i.e.  $x^{1000}$  has numerical precision issues). For this reason, we decided upon the method described in the following section.

## 3. Method for Full-Angle Scattering

### 3.1. Derivation of the New Probability Distribution Function

The purpose of this paper is to make the connection between (large-angle) single-event scattering and (small-angle) cumulative scattering. We do this in a manner that follows the methodology of Nanbu[14], but with the inclusion of single-events. This means that we will define a function  $f(\theta)$  with a known dispersion  $\bar{\mu}_f$  and set this distribution equal to the total dispersion,  $\bar{\mu}_{\text{total}}$  from (8). Here we separate the cumulative  $g(\theta)$  and single  $l(\theta)$  components, using the Heaviside function,  $H(\theta)$ , which creates a discrete transition between the two regions at the transition angle  $\theta_c$ , also described by  $\mu_c \equiv \sin^2(\theta_c/2)$ .

$$f(\theta) = g(\theta)H(\theta_c - \theta) + l(\theta)H(\theta - \theta_c) \quad (17)$$

For the cumulative portion,  $g(\theta)$ , we use a similar function to that used previously,

$$g(\theta) = \frac{\alpha_g}{2\pi s_A} \exp\left(\frac{-2 \sin^2 \frac{\theta}{2}}{s_A}\right) \quad \text{for } \theta \leq \theta_c. \quad (18)$$

We leave the normalization factor  $\alpha_g$  undefined for now; it will be solved for later to keep the entire function  $f(\theta)$  normalized to unity. Both the width and the height of this function will be modified to keep the total pdf (i.e.  $f(\theta)$ ) normalized and with the correct dispersion. This function,  $g(\theta)$ , has a total integral,  $S_g$ , and variance,  $\bar{\mu}_g$ , of

$$S_g = \alpha_g [1 - \exp(-2\mu_c/s_A)], \quad (19)$$

$$\bar{\mu}_g = \frac{s_A \alpha_g}{2} \left[ 1 - \left( 1 + \frac{\mu_c}{s_A} \right) \exp(-2\mu_c/s_A) \right]. \quad (20)$$

The single-event scattering function,  $l(\theta) = (N/\sigma_R) d\sigma_R/d\Omega$ , is

$$l(\theta) = \frac{s}{16\pi \ln \Lambda} \frac{1}{\sin^4 \frac{\theta}{2}} \quad \text{for } \theta > \theta_c \quad (21)$$



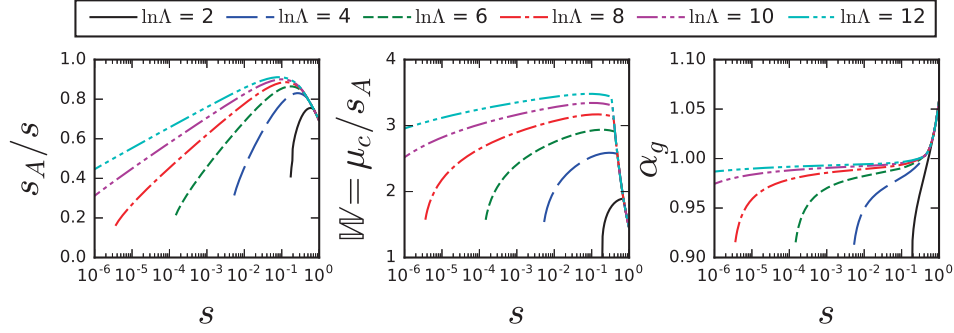


Figure 1: Values of the angular “width”,  $s_A$ , normalization factor  $\alpha_g$  of the Gaussian-like cumulative scattering region,  $g(\theta)$ , and the transition angle,  $\mu_c$ , found through solution of (27), (25) and (24) for different  $s$  and  $\ln \Lambda$ .

This function,  $l(\theta)$ , has a total integral,  $S_l$ , and variance,  $\bar{\mu}_l$ , of

$$S_l = \frac{s}{4 \ln \Lambda} \frac{1 - \mu_c}{\mu_c}, \quad (22)$$

$$\bar{\mu}_l = \frac{s}{2 \ln \Lambda} \ln \sqrt{\mu_c^{-1}}. \quad (23)$$

The total (normalized) pdf,  $f(\theta)$ , must integrate to unity (i.e.  $S_g + S_l = 1$ ). This constrains  $\alpha_g$  to

$$\alpha_g = \left(1 - \frac{s}{4 \ln \Lambda} \frac{1 - \mu_c}{\mu_c}\right) \frac{1}{1 - \exp(-2\mu_c/s_A)}. \quad (24)$$

Since we want the function to be continuous, we find the angle,  $\theta_c$ , at which these two distribution functions overlap by setting the two functions equal to each other (i.e.  $l(\theta_c) = g(\theta_c)$ ). Then we substitute  $x = -(\sin^2 \frac{\theta_c}{2})/s_A$  and take the square root of both sides to get  $\pm \sqrt{s/(8 \ln \Lambda s_A \alpha_g)} = x e^x$ . This is the Lambert W function:  $z = W_n(z) \exp W_n(z)$ . Where  $z = \pm \sqrt{s/(8 \ln \Lambda s_A \alpha_g)}$  and  $W_n(z) = x$ . For our purposes, the appropriate solution takes the  $W_{-1}$  root of the Lambert function and the negative root of the  $\pm$  under the square-root, to give the following solution,

$$\mathbb{W} \equiv \frac{\mu_c}{s_A} = -W_{-1} \left( -\sqrt{\frac{s}{8 \ln \Lambda s_A \alpha_g}} \right). \quad (25)$$

We note that for our implementation we use the rational fit method discussed in Ref. [25] to solve the Lambert function.

To match the known variance we must now find  $\bar{\mu}_f = \bar{\mu}_g + \bar{\mu}_l$ . Thus we can see that our task is to solve the following equation, where  $s$ ,  $\ln \Lambda$  are known quantities and  $s_A$ ,  $\mathbb{W}$ ,  $\alpha_g$  must be solved for:

$$\underbrace{\frac{1}{2}(1 - e^{-s})}_{\bar{\mu}_{\text{total}}} = \underbrace{\frac{s_A}{2} \left[ \frac{1 - (1 + \mathbb{W})e^{-2\mathbb{W}}}{1 - e^{-2\mathbb{W}}} \right]}_{\bar{\mu}_g} \left[ 1 - \frac{s}{4 \ln \Lambda} \left( \frac{1 - s_A \mathbb{W}}{s_A \mathbb{W}} \right) \right] + \underbrace{\frac{s}{2 \ln \Lambda} \ln \sqrt{\frac{1}{s_A \mathbb{W}}}}_{\bar{\mu}_l} \quad (26)$$

Solutions to this equation as a function of  $s$  and  $\ln \Lambda$  given the previously mentioned constraints are shown in Fig. 1. Note that the values of  $s_A/s$ ,  $\mathbb{W}$  and  $\alpha_g$  vary relatively smoothly across a large range of  $s$  values.

### 3.2. Numerical Implementation

This equation could be solved by a number of numerical solutions; we find that the following iterative method is quite simple. We solve (27) iteratively using starting values of  $s_A = s/2$  and  $\alpha_g = 1$ . As one can see from Fig. 1, these are good choices.

$$s_A = \left[ \frac{1}{1 + s/(4 \ln \Lambda)} \right] \left[ \frac{s}{4 \mathbb{W} \ln \Lambda} + \left( 1 - e^{-s} + \frac{s}{\ln \Lambda} \ln \sqrt{\frac{\mathbb{W} s_A^*}{s_A}} \right) \left( \frac{1 - e^{-2\mathbb{W}}}{1 - (1 + \mathbb{W})e^{-2\mathbb{W}}} \right) \right] \quad (27)$$



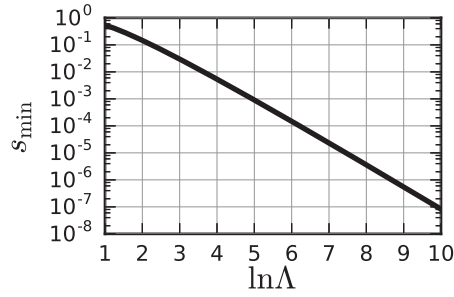


Figure 2: Minimum values of  $s$  as a function of  $\ln \Lambda$  corresponding to a single Rutherford collision event. This is the lower limit to the FAS solution, below this value a discrete Monte-Carlo scattering technique should be used.

In this equation  $s_A^*$  is the old value of  $s_A$  from the previous iteration and we take advantage of the fact that since it is underneath the logarithm its importance is reduced. At the beginning of each iteration we solve for  $\mathbb{W}$  using the right-hand-side of (25) and for  $\alpha_g$  using (24). We find that after a few iterations this method quickly converges. One could also imagine solving this equation and then creating a 2D-matrix that can be interpolated over [18] as a function of  $s$  and  $\ln \Lambda$ , which might be faster if very high accuracy is desired.

Solving this equation finds the “width”,  $s_A$ , of the spherical Gaussian function  $g(\theta)$  and the transition-angle,  $\theta_c$ ,

$$\theta_c = 2 \sin^{-1} \sqrt{\mu_c} = 2 \sin^{-1} \sqrt{s_A \mathbb{W}} \quad (28)$$

between the two distributions, from which the normalization factor  $\alpha_g$  of  $g(\theta)$  can be found. With these values the full pdf  $f(\theta)$  can be constructed. For the purpose of creating a scattering function we have inverted the normalized cumulative distribution function of  $f(\theta)$  and used the uniformly-distributed from 0 to 1, random number  $\mathcal{U}$  to give the following.

$$\cos \theta = 1 + s_A \ln \left[ 1 - \frac{\mathcal{U}}{U_c} \{1 - e^{-2\mathbb{W}}\} \right] \quad \text{for } \mathcal{U} < U_c \quad (29a)$$

$$\cos \theta = 1 - \frac{2}{(s_A \mathbb{W})^{-1} - \frac{4 \ln \Lambda}{s} (\mathcal{U} - U_c)} \quad \text{for } \mathcal{U} > U_c \quad (29b)$$

where

$$U_c = 1 - \frac{s}{4 \ln \Lambda} \left( \frac{1 - s_A \mathbb{W}}{s_A \mathbb{W}} \right) \quad (30)$$

There are two different regimes where this technique, which we now refer to as full-angle scattering (FAS), will break down. These correspond to large and small values of the transition angle,  $\theta_c$ . If  $\theta_c \geq \pi$  (i.e.  $\mu_c \geq 1$ ) then we can completely ignore the single-event scattering function  $l(\theta)$ . We could take this into account by setting  $U'_c = \max(1, U_c)$  where  $U'_c$  takes the place of  $U_c$  in (29a) and thus (29b) is not used. This is equivalent to using Nanbu’s method. However, we may run into difficulty solving for  $s_A$  when solving iteratively. We therefore propose that at value of  $s > s_{\max}$  Nanbu’s method is used, which means (12) is solved to find  $s_A = 1/A$ , and this value is used along with  $\mathbb{W} = 1/s_A$  and  $U_c = 1$  in (29a), which makes the equation identical to Nanbu’s formula in (13). As we will explain shortly, a value of  $s_{\max} = 0.5$  is appropriate for  $\ln \Lambda > 2$ .

For small  $s$ , if  $\theta_c < \theta_{\min}$  (recall that  $\theta_{\min}$  is the minimum cutoff for individual Rutherford events) then the cumulative  $g(\theta)$  must be ignored and the scattering should be done discretely. One can think of the problem this way, when  $s$  is sufficiently small then  $\bar{\mu}_l = \bar{\mu}_R$ . At this point  $\theta_c = \theta_{\min}$  and considering that  $\ln \Lambda \simeq \ln(b_{\max}/b_{\perp})$ , this means that

$$s_{\min} \simeq 4 \ln \Lambda \exp[-2 \ln \Lambda]. \quad (31)$$

This is equivalent to the particle undergoing less than a single Rutherford collision on average. So in this case we use a discrete Monte-Carlo technique that first decides if a particle will scatter using a uniformly distributed random

number  $\mathcal{U}_0$ . If the particle scatters then it is given an angle using the Rutherford differential cross-section[17]:

$$\cos \theta = 1 - \frac{2b_{\perp}^2}{b_{\perp}^2 + \mathcal{U}b_{\max}^2} = 1 - \frac{2}{1 + \mathcal{U}e^{2\ln \Lambda}} \quad \text{if } \mathcal{U}_0 < N \quad (32a)$$

Note that when  $\mathcal{U} = 0 \rightarrow \theta = \pi$ , and when  $\mathcal{U} = 1 \rightarrow \theta = \theta_{\min}$ . If  $\mathcal{U}_0$  is such that the particle does not scatter, then it does not change in angle, giving:

$$\cos \theta = 1 \quad \text{if } \mathcal{U}_0 \geq N \quad (32b)$$

### 3.3. Summary of New Full-Angle Scattering Method

To show our method in a clear and concise way, we reiterate the method using the following pseudo-code. This illustrates the three different methods that are used as a function of the normalized path-length  $s$ . At small  $s < s_{\min}$ , discrete Monte-Carlo is performed. At mid  $s$ , where  $s_{\min} < s < s_{\max}$ , our novel full-angle-scattering (FAS) method is used. Finally at high  $s > s_{\max}$  the conventional method of cumulative-only scattering[14] is used, where we have made a slight improvement to the calculation of  $\cos \theta$ . The method is designed for use in a PIC code where all of the particles will be separated in discrete partners within and between each species[13] and performed for each particle at every timestep. After determining the polar deflection angle,  $\theta$ , the azimuthal angle,  $\phi$ , is chosen randomly from 0 to  $2\pi$ .

- Calculate  $s_{\min}$  from (31)
- Set  $s_{\max}$  (we recommend  $s_{\max} = 0.5$ )
- **if**  $s < s_{\min}$  : [*Single-event only; discrete Monte-Carlo scattering*]
  - **if**  $\mathcal{U}_0 < P$  :
    - \* set  $\cos \theta$  using (32a)
  - **else** :
    - \* set  $\cos \theta$  to 1 (32b) (i.e. no scattering)
- **else if**  $s < s_{\max}$  : [*FAS; full-angle cumulative and single-event scattering*]
  - solve iteratively for  $s_A$ ,  $\mu_c$  and  $\alpha_g$  using (27), (25), and (24), respectively. Here one could imagine using a different method to solve for these variables from (26).
  - calculate  $U_c$  using (30)
  - **if**  $\mathcal{U} < U_c$  :
    - \* set  $\cos \theta$  using (29a)
  - **else** :
    - \* set  $\cos \theta$  using (29b)
- **else** (i.e.  $s \geq s_{\max}$ ) : [*COS; Cumulative-only scattering*]
  - solve for  $s_A = 1/A$  using (12) (i.e. Nanbu's method)
  - \* set  $\cos \theta$  using (13)

Now that we have defined this methodology, we next compare it to discrete Monte-Carlo simulations that model each Rutherford collision individually to verify that our method produces this exact result.

### 3.4. Benchmarking Against Discrete Monte-Carlo Scattering Results

We set up a stochastic discrete Monte-Carlo scattering (DMCS) method to verify that our FAS algorithm produces a pdf that is consistent with the accumulation of many single scattering events. This method first determines the probability of a Rutherford collision  $P_R = \sigma_R n_j v_{ij} dt$ . The algorithm then determines a random number  $\mathcal{U}_0$ ; if  $\mathcal{U}_0 > P_R$  the nothing happens; if  $\mathcal{U}_0 < P_R$  then the particle is scattered into

$$\cos \theta = 1 - \frac{2b_{\perp}^2}{b_{\perp}^2 + \mathcal{U}_1 b_{\max}^2}, \quad (33)$$

where  $\mathcal{U}_1$  is another random number. The azimuthal angle,  $\phi$ , is chosen uniformly from 0 to  $2\pi$ . This is identical to the method used in our new scattering algorithm if  $s < s_{\min}$  and is the method that we are trying to reproduce with our FAS approach at large timesteps. The DMSC simulation was run with a timestep such that the probability for a single Rutherford collision was 0.01; we confirmed that the timestep was adequate through convergence testing. All of the simulations (both DMCS and the FAS method) are set up as two colliding streams of cold particles. One of these species of particles is followed and evolves over time (H ions,  $A=1$ ,  $Z=1$ ), and the other ions are used for scattering but are not modified during each timestep (C ions,  $A=12$ ,  $Z=1$ ). Self-collisions within the streams are not included to allow us to focus only on a single type of collision (i.e. H with C). The ion density is  $5 \times 10^{22} \text{ cm}^{-3}$  per stream; and the Coloumb logarithm is found using  $\ln \Lambda = \frac{1}{2} \ln \left[ (b_{\max}^2 + b_{\perp}^2) / b_{\perp}^2 \right]$ , with the maximum impact parameter,  $b_{\max}$ , set to the Debye length,  $\lambda_D = \sqrt{\epsilon_0 T_e / (n_e q_e^2)}$ , with  $T_e = 500 \text{ eV}$ . We set the velocities of the H,  $v_H$ , and the C,  $v_C$ , ions such that the laboratory frame-of-reference is the center-of-mass frame. Unless noted, the simulations were run with  $5 \times 10^6$  macro-particles in each ion stream.

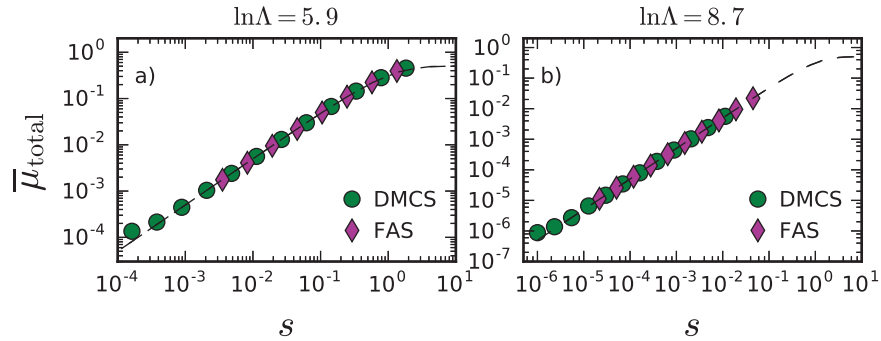


Figure 3: Plot of  $\bar{\mu}_{\text{total}}$  for the Monte-Carlo (circles) and our FAS method (diamonds) compared with the analytical equation from Nanbu, i.e. (8):  $\bar{\mu}_{\text{total}} = \frac{1}{2}(1 - e^{-s})$ . The two plots are for a)  $\ln \Lambda = 5.9$  and b)  $\ln \Lambda = 8.7$ . We note that at  $s = 1$ ,  $t = 2.3 \times 10^{-4} \text{ ns}$  and  $t = 1.0 \times 10^{-2} \text{ ns}$  for the  $\Lambda = 5.9$  and  $\ln \Lambda = 8.7$  cases, respectively.

To be clear, as we move into physical parameters, the parameter  $s$  can be thought of as both normalized-path or a normalized collision-time. That is,  $s = t/\tau_{ij} = L/\lambda_{ij}$ , where  $t$  is the physical time (e.g. ns),  $L$  is the physical length,  $\tau_{ij}$  is the inverse slowing-down collision frequency [3],

$$\tau_{ij} = \frac{4\pi\epsilon_0^2 m_{ij}^2 v_{ij}^3}{q_i^2 q_j^2 n_j \ln \Lambda} \quad (34)$$

and  $\lambda_{ij} = v_{ij}\tau_{ij}$  is the collisional mean-free-path for species  $i$  on species  $j$ . We recall using Nanbu's method on similar mass species requires a resolution of  $\tau_{ij}$  by a factor of 100[24, 23], thus indicating a that required timestep for COS collisions would be  $s = 10^{-2}$ . However, one must be careful when comparing the required COS timestep to the one required for FAS. By definition, the fact that single-event collisions are of interest means that the physical system is evolving on timescales that are faster than  $\tau_{ij}$ .

Two sets of parameters were run to look at different verifications of our method. 1)  $\ln \Lambda = 5.9$ , where  $v_H = 250 \text{ km/s}$  and  $v_C = 20.8 \text{ km/s}$  was run to look at longer times when the pdf becomes isotropic. The smaller value of

the Coluomb logarithm makes this possible. 2)  $\ln \Lambda = 8.7$ , where  $v_H = 1000$  km/s and  $v_C = 83.3$  km/s. This setup was used to show when single-events are very important. Due to computational expense, it was not possible to run simulations with the smallest timestep until isotropic. We note that these simulation are set up to verify our method when  $s_{\min} < s < s_{\max}$ , which is the newest portion of our method and thus the most important to verify.

First, we have confirmed the formula for increasing angular variance,  $\bar{\mu}_{\text{total}}$ , over time from Nanbu's paper. As shown in Fig. 3 we find excellent agreement between the DMCS results (circles) and the analytical solution from (8) (dashed line) for both  $\ln \Lambda = 5.9$  and  $\ln \Lambda = 8.7$ . We repeated this exercise using the FAS method (diamonds) and also find excellent agreement, which verifies that our method does what we designed it to do.

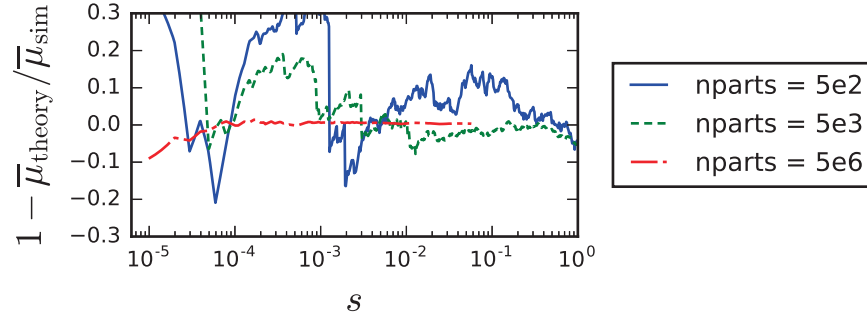


Figure 4: Errors of the FAS simulations' angular variance,  $\bar{\mu}_{\text{sim}}$ , versus theoretical angular variance,  $\bar{\mu}_{\text{theory}}$ , for different numbers of macro-particles.

We investigate using a low number of macro-particles to see if as low as 500 particles introduces any systematic error into the FAS method. The results are plotted in Fig. 4 as the error between the simulation,  $\mu_{\text{sim}}$ , and the expected value,  $\mu_{\text{theory}}$ , from (8). These results show that the random error is larger with fewer particles; however this error seems to be random, meaning that it fluctuates around the zero. We do not see evidence of systematic error when using fewer particles. This means that while a lower particle number may not properly resolve the pdf, it will not introduce systematic numerical errors. This suggests that under-resolving the particle number may not recover the correct pdf, but should still give the correct transport and equilibration properties. However, one should be wary of under-resolving these simulations and should perform a convergence study increasing the number of macro-particles until a stable result is attained.

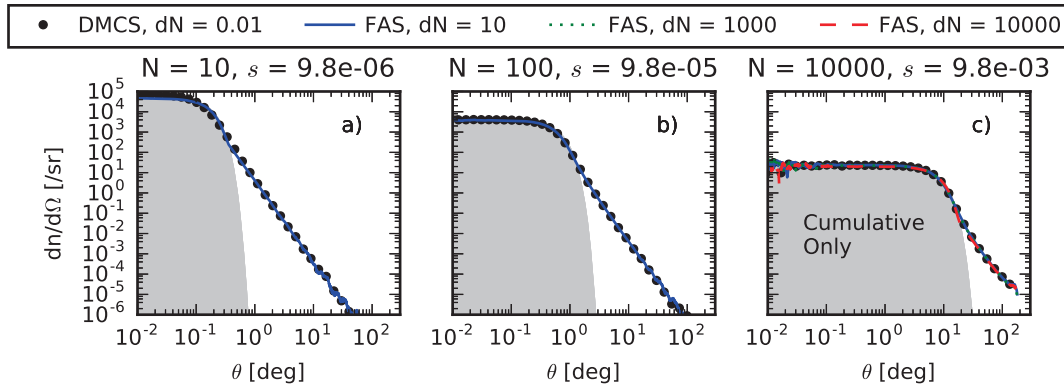


Figure 5: Plot of the normalized probability distribution functions (pdf) of the Monte-Carlo result (circles) and our new method (line) for different normalized times,  $N$ . The pdf from Nanbu[14] (COS) is plotted as a shaded region. Here  $N = \sigma_R v_{ij} n_j dt$  is the number of single-event (Rutherford) collisions. We note that “by eye” it may seem that the COS results do not have the same area under the curve and variance as the other results; this is an appearance due to the logarithmic scale, as the slight increase in the COS pdf at small angles is not visible.

The main purpose of our new method is to capture the correct pdf for the entire range of angles at all times. As

the pdf covers a large range of angles and magnitudes, we have plotted both log-log (Fig. 5) and linear-linear (Fig. 6) plots. The log-log plots in Fig. 5 show how the FAS method (lines) correctly captures the large-angle behavior of the pdf compared to the DMCS simulation (circles). The fact that the FAS method matches at large angles is not a surprise, because these large angles are dominated by single-events and have essentially the same (Rutherford) cross-section in both the DMCS and FAS method. This plot also shows how using cumulative-only scattering (shaded grey fill) greatly underestimates the pdf at large angles.

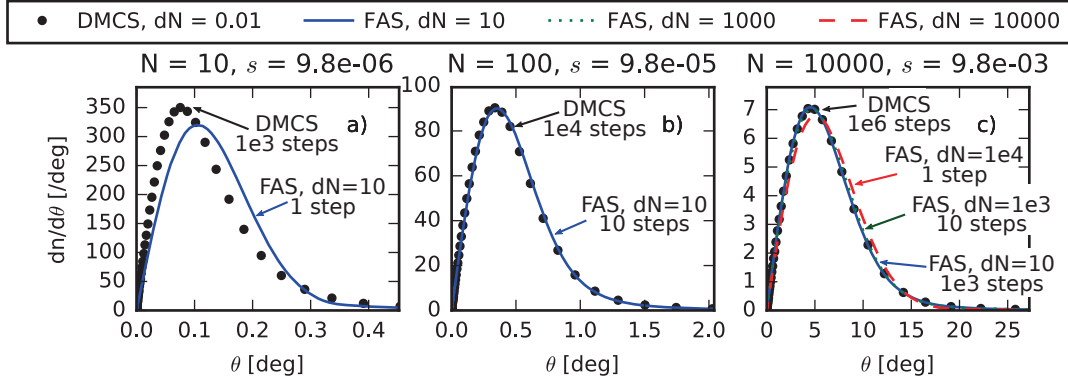


Figure 6: Plot of the normalized probability distribution functions (pdf) of the Monte-Carlo result (circles) and our new method (line) for different normalized times,  $N$ . Here  $N = \sigma_{RV_{ij}n_j dt}$  is the number of single-event (Rutherford) collisions.

The linear plots in Fig. 6 look into more detail at how the pdfs match at small angles. Here we plot the number of particles per angle ( $dn/d\theta$ ), as this better represents the total number of particles and thus how good the fit is, compared to the number of particles per steradian ( $dn/d\Omega$ ). In Fig. 6a the Monte-Carlo method has run for  $10^3$  timesteps and our new method (w/  $dN = 10$ ) has run for only one timestep. At this point, the two simulations do not agree exactly. This suggests that our method is not “perfect”; that is we do not precisely capture the transition from cumulative to single-event scattering in a single timestep. This is logical, as our method enforces a discrete transition from cumulative to single-event scattering, while the true pdf blends the two regions together smoothly. However, as shown in Fig. 6b after 10 timesteps our method (w/  $dN = 10$ ) converges towards the correct solution. This shows that while our method is not perfect on the first timestep, it is accurate at convergence and thus is able to reproduce the correct pdf after  $\sim 10$  timesteps. This suggests that for a given FAS model to work it is not necessary to capture the transition region precisely; instead it should arise naturally from the algorithm itself. This works because the single-events will blend into the cumulative distribution function over longer times as a consequence of the central limit theorem. In Fig. 6c, we plot three simulations:  $dN = 10$ ,  $dN = 10^3$ ,  $dN = 10^4$  at  $N = 10^4$ . This plot shows that both  $dN = 10$  and  $dN = 10^3$  have converged to the DMCS solution, while  $dN = 10^4$  has not. This is consistent with the previous times, as both  $dN = 10$ ,  $dN = 10^3$  have run for 10 or more timesteps and  $dN = 10^4$  has only run for a single timestep. To quantify the convergence of our method we use the  $R^2$  method[26], where  $R$  is defined as

$$R = \frac{\sum (O_i - \bar{O})(E_i - \bar{E})}{\sqrt{\sum (O_i - \bar{O})^2 \sum (E_i - \bar{E})^2}} \quad (35)$$

where,  $O_i$  is the number of macro-particles in the bin  $i$  for the observed quantity (i.e. the FAS distribution) and  $E_i$  refers to the expected quantity (i.e. the DMCS distribution); the “barred” variables (e.g.  $\bar{O} = \sum O_i/N$ ) are averages, where  $N$  is the total number of bins. The significance of the correlation between the two distributions increases as  $R^2$  approaches unity from zero. We also use the chi-squared test[26], where the reduced chi-squared,  $\tilde{\chi}^2$ , is defined as

$$\tilde{\chi}^2 = \frac{1}{N-1} \sum \left( \frac{O_i - E_i}{\sqrt{O_i + E_i}} \right)^2. \quad (36)$$

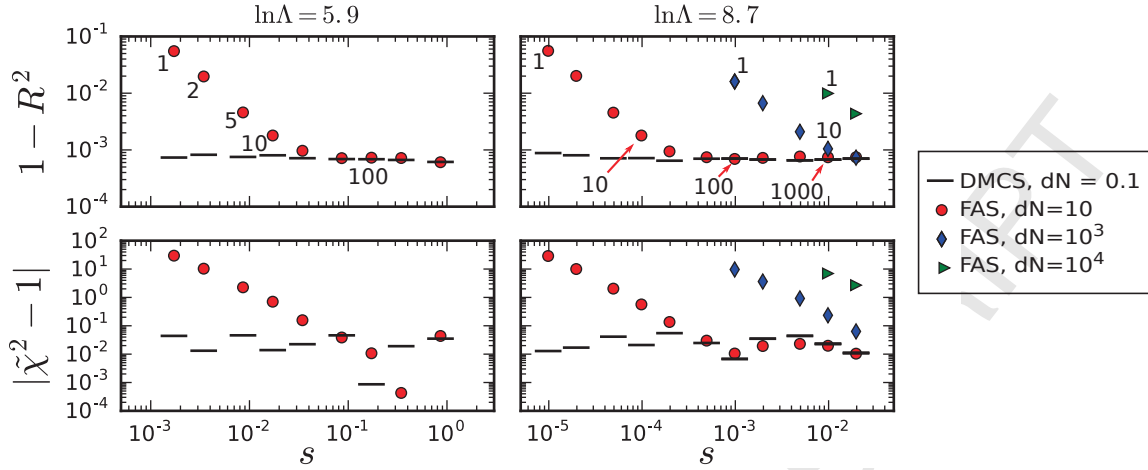


Figure 7:  $R^2$  (top) and  $\tilde{\chi}^2$  (bottom) methods for understanding agreement between the DMCS and the FAS methods as a function of  $s$  for values of  $\ln \Lambda = 5.9$  (left) and  $\ln \Lambda = 8.7$  (right). The horizontal line points represent two DMCS simulations compared against each other to understand the disagreement based on noise. The other points represent FAS simulations with  $dN = 10$  (circles),  $dN = 10^3$  (diamonds) and  $dN = 10^4$  (triangles). The numbers on the graphs show the correspond to the number of timesteps for each run; points are placed at intervals of : 1, 2, 5, 10, 20, 50, etc. We find that for around 10–20 timesteps the FAS method converges to within the noise.

Here the significance of the correlation between the two distributions increases as  $\tilde{\chi}$  approaches unity from infinity. Both the  $R^2$  and  $\tilde{\chi}^2$  methods show how well the two distributions agree, but are slightly different in that the  $R^2$  uses an empirical method to determine the deviation of values (i.e. denominator in (35)) and  $\tilde{\chi}^2$  uses the expected sampling error (i.e. denominator after sum in (36)). Both tests, for different values of  $\ln \Lambda$ , are plotted in Fig. 7, where we subtract unity from the squared values to allow plotting on a logarithmic scale. Different values of the timestep  $dN$ , as circles ( $dN = 10$ ), diamonds ( $dN = 10^3$ ) and triangles ( $dN = 10^4$ ) are shown. Clearly values closer to zero represent better agreement between the simulations, however it is not clear from this magnitude alone when the agreement is “good enough.” For this reason, we ran a second set of identical DMCS simulations and performed the  $R^2$  and  $\tilde{\chi}^2$  test on this; the results are plotted as thick horizontal lines in Fig. 7. These values represent the different in the two distributions due to noise alone, thus once the FAS simulations reach this level they can be considered identical to the DMCS runs. Therefore, as we expect qualitatively from Fig. 6, we see that after 10 to 20 timesteps the FAS method converges to the desired DMCS results. We note that in a full-scale simulation, this does not necessarily mean that a FAS simulation must be resolved 20 times better than an equivalent COS simulation, because other physics often govern timestep resolution. For instance, in PIC plasma simulations, the timescale of electro-magnetic propagation or the plasma frequency may be much smaller than collisional timescales. Additionally, only one species of particle may have FAS features of interest (e.g. ions), while the higher collisionality of another species (e.g. electrons) governs the required collisional resolution.

The time saving from the FAS method compared with DMCS is substantial. For example, the  $\ln \Lambda = 8.7$  case (5e6 macro-particles; 16 total cpu-cores) took  $10^6$  seconds for the DMCS run ( $dN = 0.01$ ),  $2 \times 10^5$  seconds for the FAS with  $dN = 10$ , and  $2 \times 10^3$  seconds with  $dN = 10^3$  to reach the point of  $s = 10^{-2}$  at which point all of the simulations were converged. Thus for a simulation requiring a time resolution of  $dt/\tau_{ij} = 10^{-2}$ , the time savings would be a factor of 500 with no loss of accuracy by using the FAS method compared to DMCS. On the other hand, the COS simulation of  $dN = 10^4$  took only  $9 \times 10^2$  seconds; a factor of more than 2x faster than the equivalent FAS run. However, these tests focus on the scattering method alone and exclude many aspects of a fullscale simulation (e.g. particle advancement, particle sorting, electro-magnetic waves) and thus over-estimate the cost of FAS in practice. In Section 4, we show the implementation of the FAS method in a PIC code for different system of interest. In these tests, we find a 20% increase in computational time compared to COS. Additionally, we mention that a companion Article to this one[18] uses a table lookup, in contrast to our iterative solve method, and has the potential to increase computational speed.



### 3.5. Regimes of Interest for Full-Angle Scattering

We now provide more context so that a code developer or user can determine if including full-angle scattering is of importance to their problem of interest. First, we look at the contribution to angular variance due to cumulative,  $\bar{\mu}_g$ , and single-events,  $\bar{\mu}_l$  with respect to the total angular variance,  $\bar{\mu}_{\text{total}}$ . As the number of scattering events increases, both the transition angle,  $\theta_c$ , and the width of  $g(\theta)$  increase; this causes the relative importance of single-events to decrease. Fig. 8 shows this quantitatively by plotting the ratio of cumulative to total angular variance ( $\bar{\mu}_g/\bar{\mu}_{\text{total}}$ ), where  $\bar{\mu}_g$  is found from the first term on right-hand-side of (26). This plot shows how the importance of single-events ( $\bar{\mu}_l = \bar{\mu}_{\text{total}} - \bar{\mu}_g$ ) decreases with  $s$ . This plot also justifies the use of a  $s_{\text{max}} = 0.5$ , as the transition point when the effect of single-events can be ignored and cumulative scattering dominates. In the same sense, a simulation where the timescales of interest are much larger than  $s = 0.5$  including full-angle scattering is probably not necessary.

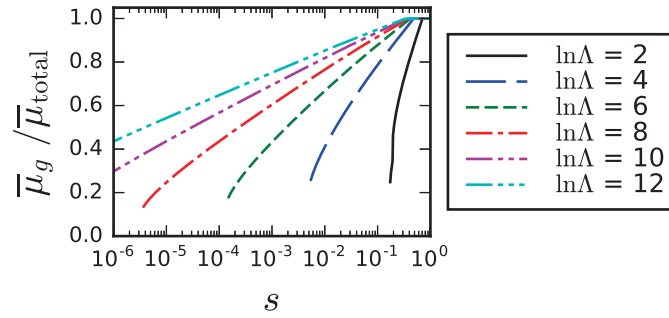


Figure 8: Relative importance of the angular variance,  $\bar{\mu}_g$ , of the Gaussian-like cumulative pdf  $g(\theta)$  compared with total angular variance,  $\bar{\mu}_{\text{total}}$ .

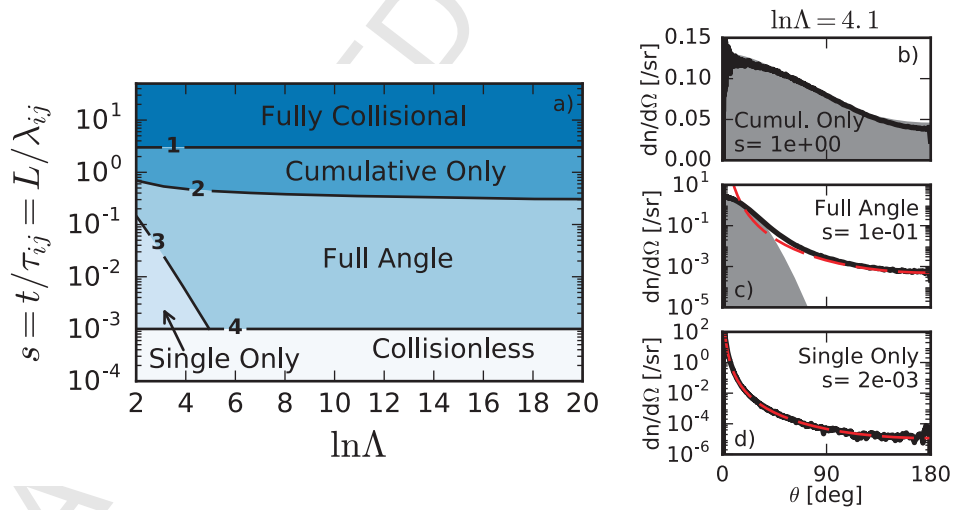


Figure 9: a) A chart of different scattering regimes of interest. Line-1 corresponds to  $\bar{\mu}_{\text{total}} = 0.95/2$  ( $s \approx 3$ ), line-2 to  $\mu_c = 0.99$ , line-3 to  $s = s_{\text{min}}$  and line-4 to  $s \approx 2\bar{\mu}_{\text{total}} = 10^{-3}$ . We note that in this case  $s$  corresponds to the physical time/length of interest in the system and not the timestep of the simulation. Panels on the right show representative pdfs of regimes of b) cumulative only scattering, c) full-angle scattering and d) single-event only scattering for a DMCS simulation of  $\ln \Lambda = 4.1$  at  $s = 2.4 \times 10^{-3}$ ,  $1.0 \times 10^{-1}$  and  $1.5$ , respectively. The solid line shows the simulation, the filled curve shows the cumulative portion and the dashed line shows the single-event portion.

To put full-angle scattering in a larger context of scattering in plasmas we have created the chart in Fig. 9a that indicates five regimes of scattering as a function of the normalized path-length  $s$  and  $\ln \Lambda$ . We note that in this case  $s$  refers to the physical time/length of interest in the system and not the timestep. For instance, timesteps in the



“collisionless” regime may at times be needed to resolve single-event only or full-angle scattering. The different regimes are separated by four lines: Line-1 indicates the regime where scattering transitions to isotropic; above this line the cumulative pdf is so broad that becomes flat. We define this line as  $\bar{\mu}_{\text{total}} = 0.95/2$  (i.e.  $s \approx 3$  from (8)), recalling that with completely isotropic scattering  $\bar{\mu}_{\text{total}} = 1/2$ . Line-2 is the transition point at which cumulative scattering overtakes single-event scatters even at the largest scattering angles. Above this line we expect a pdf that looks similar to Fig. 9b and below we expect a pdf as in Fig. 9c. This line is defined as when  $\mu_c = 0.99$  and thus transition-angle,  $\theta_c$  of  $168.5^\circ$ . Line-3 defines the transition to where cumulative collisions exist, below this line the cross-section for single-events is so low that not enough collisions will have accumulated and we expect a pdf as shown in Fig. 9d. This line is defined as when the transition angle,  $\theta_c$ , is equal to the Rutherford cutoff angle,  $\theta_{\min}$ , or equivalently when  $s = s_{\min}$  from (31). Line-4 indicates the transition to a collisionless regime. If the particles have a very low normalized path-length then collisions are likely unimportant. We define this line as when  $s \approx 2\bar{\mu}_{\text{total}} = 10^{-3}$ . Using this chart, with known values of the times/lengths of interest and the Coulomb logarithm, one can get a general idea of what regime of scattering may be of interest to the problem at hand.

#### 4. Physical Systems of Interest

In order to show the importance of including the single-events scattering into a physical system we run two types of simulations to test 1) interpenetration of plasma streams and 2) temperature equilibration between two ion species. In both of these systems, we focus on the neutron production from deuterium, since the DD cross-section is strongly dependent on the relative velocity,  $v_{ij}$ , between the two fusing deuterons. Our new FAS method generates ions in the wings of the pdf that, though low in number, have a larger fusion cross-section and modify the neutron production in both yield and spectrum. We note that for these following runs the FAS method increases the computation expense by around 20%.

##### 4.1. Interpenetrating Plasma Flows

The first test setup is similar to experiments on the National Ignition Facility (NIF) focused on interpenetrating plasmas[16]. Here we simulate two opposing flows in a symmetric box of CD and CH. Each ion species is initialized with a temperature of 1 keV; a density of  $2.86 \times 10^{19} \text{ cm}^{-3}$ ; an ionization state of  $Z = 6$  for carbon; and a velocity of  $\pm 1000 \text{ km/s}$  (CD flows in the positive and CH in the negative z-direction). The slowing-down mean-free-paths,  $\lambda_{ij}$ , (calculated from eqn. (7.42) in Ref. [3]) are 6.5 and 19.10 mm, and slowing-down times,  $\tau_{ij} = \lambda_{ij}/v_{ij}$ , are 3.3 and 9.6 ns for C-C and D-C, respectively. The simulations are run with the particle-in-cell (PIC) code LSP[27] without any electro-magnetic fields. We run simulations with our new FAS scattering model and compare these with the conventional cumulative-only scattering (COS) method from Nanbu[14]. As shown in Fig. 10, bulk quantities such as the deuteron bulk velocity (Fig. 10a) and temperature (Fig. 10b) are the same independent of scattering model. This is expected; our FAS method explicitly constrains the energy exchange cross-section ( $\propto \sin^2[\theta/2]$ ) to be the same in both methods and thus the consistency between the two methods can be seen as a type of verification. However, unlike the bulk quantities of temperature and velocity, the neutron yield is dramatically changed as shown in the ratio plot (yield-of-FAS divided by yield-of-COS) shown in Fig. 10c. This indicates that despite having the same temperature with both scattering models, the distribution function of the deuterons is changed in such a way to alter the neutron production at early times in the interpenetration.

Figure 11 shows in detail both the deuteron and carbon z-velocity pdfs. One can see that at early times (0.2 ns; Fig. 11b,e) the FAS method creates a significant variation of the wings of both the deuterium and carbon pdfs. At this point in time, the neutron yield is about 3x higher using FAS. These wing (i.e. deviations from the Maxwellian) are the cause of the increase of neutron production, because the neutron production happens at the Gamow peak and, at this point in time, these wings dramatically increase the number of ions at this peak. However, by 1 ns, the neutron yield ratio has dropped back to unity, despite the fact that we still seem a difference in the deuteron pdf at this time (Fig. 11c). The reason for this, as shown previously in Fig. 8, is that as the number of scattering events increase, the importance of single-event scattering decreases. This can be seen in how the temperature of the deuterons broadens the velocity pdf and overtakes the single-event collisions. Thus the velocity of peak neutron production (i.e. Gamow peak) is dominated by the bulk of the pdf and no longer the non-Maxwellian wings.

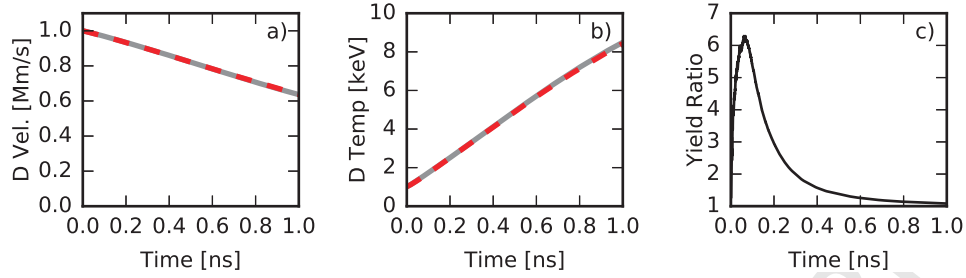


Figure 10: Bulk quantities from interpenetrating flow simulations with our new FAS model as a dashed line and the COS model as a solid line. a) Deuteron bulk velocity, b) deuteron temperature, and c) ratio of neutron yield in the new FAS method compared to that of the COS method. Here  $\tau_{CC} = 3.3$  ns and  $\tau_{DC} = 9.6$  ns.

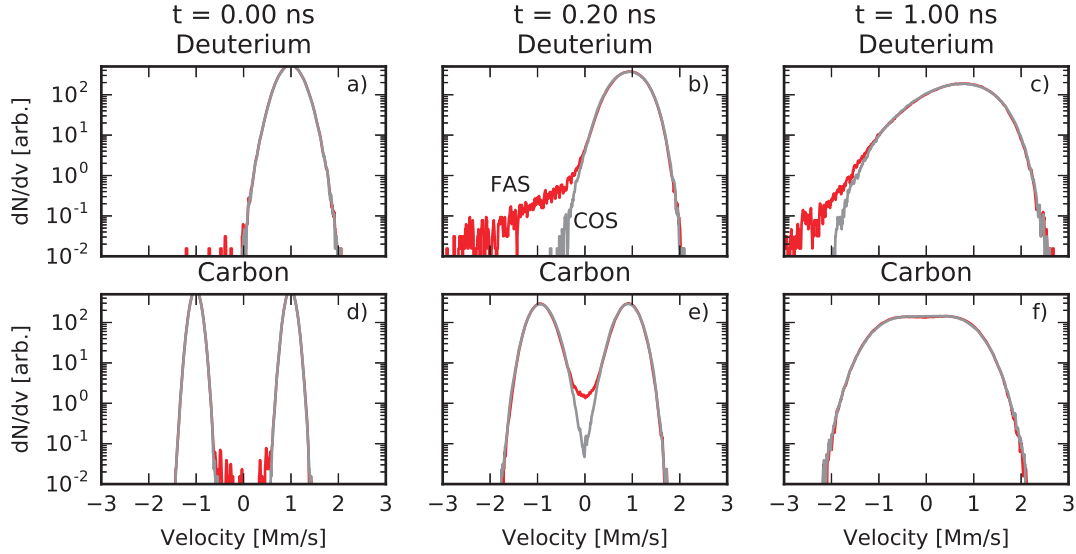


Figure 11: Deuteron (a-c) and carbon (d-f) z-velocity distribution functions at times 0 (a,d), 0.2 (b,e) and 1.0 ns (c,f). Our new FAS model is shown as the darker line and the conventional COS method is shown as a light gray line as labeled in (b).

From these simulations it is clear that including the effect of single-event scattering is of fundamental importance to capturing experimental observables (e.g. neutron yield) in interpenetrating plasma flow experiments. These effect will be most dominant when the system size is on the order of, or greater than, the mean-free-path of the ion species.

#### 4.2. Temperature Equilibration

To make a connection with previous work from Turrell, Sherlock and Rose[17], we model a system as it goes through temperature equilibration. While not directly related to inertial confinement fusion (ICF) due the lower densities and different ion species, it provides some intuition on how such systems evolve and how bulk neutron quantities such as the excess kurtosis will change due to single-event scattering. We initialize the simulations as a CD plasma, where both ion species have a density of  $2.86 \times 10^{19} \text{ cm}^{-3}$ ; the carbon ions ( $Z = 6$ ) are initialized with a temperature of 5 keV; and the deuterons with a temperature of 0.5 keV. There is no bulk motion of the plasma. The Coloumb logarithm is calculated as  $\ln \Lambda = 9.2$ . The temperature equilibration timescale[22],  $\tau_{ij}^E$ ,

$$\tau_{ij}^E = \frac{6\pi^{3/2} \epsilon_0^2 m_i m_j v_{th}^{3/2}}{\sqrt{2} q_i^2 q_j^2 n_j \ln \Lambda} \quad (37)$$

where  $v_{th} \equiv \sqrt{(T_i/m_i + T_j/m_j)}$  with  $T$  representing temperature, is  $\tau_{DC}^E = 0.4$  ns.

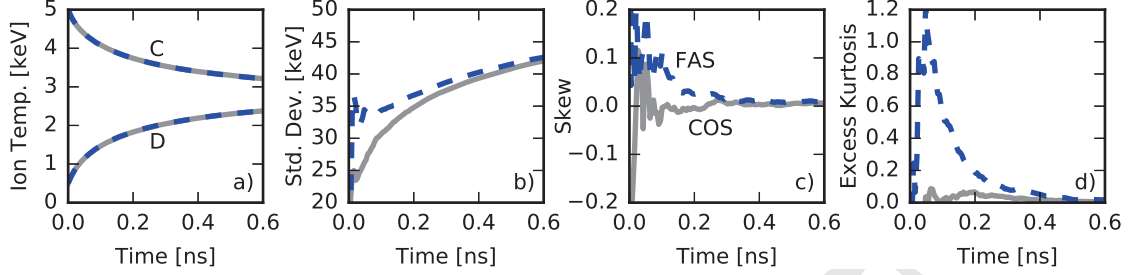


Figure 12: Quantities from temperature equilibrium simulations with our new FAS model as a dashed line and the conventional COS model as a solid line. a) Carbon (top lines) and deuteron (bottom lines) temperatures, b) neutron energy standard deviation,  $\sigma_n$ , c) neutron skew,  $\mathcal{S}$ , and d) neutron excess kurtosis,  $\kappa$ . Here the temperature equilibration timescale,  $\tau_{DC}^E$  is 0.4 ns.

Figure 12a shows the temperature equilibration of the two species for both the new FAS technique (dashed line) and the COS method from Nanbu[14]. As in the previous system, the two scattering methods agree well in terms of this bulk fluid quantity. Additionally, we find that the neutron yield with our new FAS model only increases by a maximum of 20% and is less than 5% greater at 0.3 ns. However, there are still changes in the neutron spectral shape which may be interesting considering that such shapes are used to diagnose implosions on NIF to understand the bulk velocity variance within the capsule[28, 29]. To quantify the shape of the neutron spectrum, the average energy of the normalized neutron energy spectrum  $f(E)$ ,  $E_0$ , is defined as  $E_0 = \int E f(E) dE$ . The standard deviation,  $\sigma_n$ , which defines the width of the spectrum, is defined as

$$\sigma_n^2 = \int (E - E_0)^2 f(E) dE, \quad (38)$$

the skew,  $\mathcal{S}$ , which defines if the distribution is asymmetric to either direction is defined as

$$\mathcal{S} = \sigma_n^{-3} \int (E - E_0)^3 f(E) dE, \quad (39)$$

and, finally, the kurtosis,  $\tilde{\kappa}$ , is defined as

$$\tilde{\kappa} = \sigma_n^{-4} \int (E - E_0)^4 f(E) dE, \quad (40)$$

and the excess kurtosis,  $\kappa$ , as  $\kappa = \tilde{\kappa} - 3$ . The excess kurtosis of a Gaussian distribution function is zero, meaning that the excess kurtosis is a measure of the amount a given pdf differs from a Gaussian pdf.

The standard deviation of the neutron spectrum (Fig. 12b) is only slightly modified by the scattering model. This is expected, as this measurement is closely associated with the bulk deuteron temperature, which is relatively unaffected by our new method. However, both the skew (Fig. 12c) and the excess kurtosis (Fig. 12d) of the neutron spectrum are changed when using FAS when the temperature difference between deuteron and carbon species is high. This finding is in agreement with the work done in Ref.[17], which found that excess kurtosis was generated in simulations that included large-angle collisions when heating a DT (deuterium-tritium) plasma with alpha particles.

In Fig. 13, we show the deuteron and neutron energy pdf at early time (0.11 ns, Fig. 13a,b) when the temperatures are far apart and later in time (0.6 ns, Fig. 13c,d) when the ions have had longer to equilibrate. At early times, we find that including single-events creates a large tail in the deuteron distribution and thus creates long wings in the neutron energy pdf, which can be seen as excess kurtosis in Fig. 12d. At later times, the effect of these single event collisions is over-shadowed by the multiple-collisions and the kurtosis on the neutron pdf likewise vanishes. While this test problem is done with different species and at different conditions than an ICF implosion, it highlights another possibility for adding kurtosis to the system that is unrelated to bulk velocity variance. Therefore, when a system lacks equilibration between ion species, such effects should be accounted for.

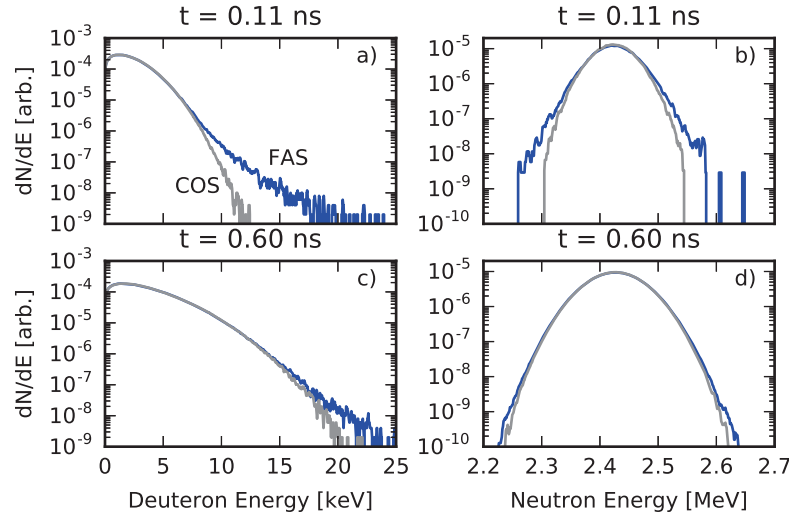


Figure 13: Deuteron (a,c) and neutron (b,d) energy distribution functions at times 0.11 (a,b) and 0.60 ns (c,d) from temperature equilibrium simulations. Our new FAS model is shown as the darker line and the COS method is shown as a light gray line as labeled in (a).

## 5. Summary

In situations where the particle mean-free-path is relatively large it may be necessary to accurately model the complete accumulated angular distribution of scattered particles. In conventional, small-angle, cumulative-only scattering (COS) methods, single-event scattering is ignored and the distribution under-estimates the scattering at large angles. In this Article, we have developed a self-consistent, full-angle-scattering (FAS) method for use in particle-in-cell plasma simulations and verified it against discrete Monte-Carlo scattering (DMCS) calculations. We find that even with relatively large timesteps our algorithm converges on the DMCS results at vastly reduced computational expense. We have outlined the limits of the FAS method as a function of the normalized path-length  $s$  and suggest using DMCS and COS methods at limits of small and large  $s$ , respectively. Additionally, two different physical systems were analyzed to study the effects of single-event scattering. The effects on neutron yield and spectrum were found to be dramatically altered through including of our new FAS method as compared with conventional COS.

## Acknowledgments

The importance of including large-angle-scattering in interpenetrating plasmas was suggested by Dr. D. D. Ryutov. We acknowledge insightful discussion with Drs. J. R. Angus, B. Cohen, A. Dimits, A. Link, M. Sherlock and S. C. Wilks. This work was performed under the auspices of the U.S. Department of Energy by Lawrence Livermore National Laboratory (LLNL) under Contract DE-AC52-07NA27344. Support was provided by the LLNL Laboratory Directed Research and Development Program (LDRD) 15-ERD-065 (PI: Dr. J. S. Ross) and from the SC-FES High Energy Density Laboratory Plasmas (HEDLP) program (PI: Dr. H.-S. Park). Computing support for this work came from the LLNL Institutional Computing Grand Challenge.

## References

- [1] G. Molière, Theorie der streuung schneller geladener teilchen II: Mehrfach- und vielfachstreuung [Theory of scattering of rapidly charged particles II: Multiple and multiple scattering], Z. Naturforsch 3a (1948) 78.
- [2] H. Bethe, Molière's theory of multiple scattering, Phys. Rev. 89 (6) (1953) 1256.
- [3] B. Trubnikov, Particle interactions in a fully ionized plasma, Rev. Plasma Phys. 1 (1965) 105.
- [4] J. D. Jackson, Classical Electrodynamics, John Wiley and Sons, 1999.
- [5] M. J. Berger, et al., Monte carlo calculation of the penetration and diffusion of fast charged particles, Methods in computational physics 1 (1963) 135–215.

- [6] I. Kawrakow, Accurate condensed history monte carlo simulation of electron transport. i. egsrc, the new egs4 version, *Medical physics* 27 (3) (2000) 485–498.
- [7] D. W. O. Rogers, Fifty years of monte carlo simulations for medical physics, *Physics in Medicine and Biology* 51 (13) (2006) R287.
- [8] S. Goudsmit, J. Saunderson, Multiple scattering of electrons, *Physical Review* 57 (1) (1940) 24.
- [9] S. M. Seltzer, An overview of etran monte carlo methods, *Monte Carlo Transport of Electrons and Photons* 38 (1988) 153–181.
- [10] J. Halbleib, R. Kensek, T. Mehlhorn, G. Valdez, S. M. Seltzer, M. J. Berger, Its version 3.0: the integrated tiger series of coupled electron/photon monte carlo transport codes, SAND91-1634.
- [11] J. F. Briesmeister, Mcnp-a general monte carlo n-particle transport code, version4a, LA-12625.
- [12] W. R. Nelson, H. Hirayama, D. W. Rogers, Egs4 code system, Tech. rep., Stanford Linear Accelerator Center, Menlo Park, CA (USA) (1985).
- [13] T. Takizuka, H. Abe, A binary collision model for plasma simulation with a particle code, *Journal of Computational Physics* 25 (3) (1977) 205–219.
- [14] K. Nanbu, Theory of cumulative small-angle collisions in plasmas, *Phys. Rev. E* 55 (4) (1997) 4642.
- [15] A. Thomas, M. Tzoufras, A. Robinson, R. Kingham, C. Ridgers, M. Sherlock, A. Bell, A review of vlasov–fokker–planck numerical modeling of inertial confinement fusion plasma, *Journal of Computational Physics* 231 (3) (2012) 1051–1079.
- [16] J. S. Ross, D. P. Higginson, D. Ryutov, F. Fiuza, R. Hatarik, C. M. Huntington, D. H. Kalantar, A. Link, B. B. Pollock, B. A. Remington, et al., Transition from collisional to collisionless regimes in interpenetrating plasma flows on the national ignition facility, *Phys. Rev. Lett.* 118 (18) (2017) 185003.
- [17] A. E. Turrell, M. Sherlock, S. J. Rose, Self-consistent inclusion of classical large-angle coulomb collisions in plasma monte carlo simulations, *J. Comp. Phys.* 299 (2015) 144–155.
- [18] B. I. Cohen, D. P. Higginson, C. D. Eng, W. A. Farmer, A. Friedman, D. P. Grote, D. J. Larson, Monte carlo calculation of large and small-angle electron scattering in air, submitted to *J. Comp. Phys.*
- [19] K. Nanbu, Momentum relaxation of a charged particle by small-angle coulomb collisions, *Phys. Rev. E* 56 (6) (1997) 7314.
- [20] J. Fernández-Varea, R. Mayol, J. Baró, F. Salvat, On the theory and simulation of multiple elastic scattering of electrons, *Nuclear Instruments and Methods in Physics Research Section B: Beam Interactions with Materials and Atoms* 73 (4) (1993) 447–473.
- [21] H. W. Lewis, Multiple scattering in an infinite medium, *Phys. Rev.* 78 (5) (1950) 526.
- [22] L. Spitzer Jr., *Physics of Fully Ionized Gases*, 2nd Edition, Dover Books on Physics, 2006.
- [23] A. M. Dimits, C. Wang, R. Caflisch, B. I. Cohen, Y. Huang, Understanding the accuracy of nanbu’s numerical coulomb collision operator, *J. Comp. Phys.* 228 (13) (2009) 4881–4892.
- [24] C. Wang, T. Lin, R. Caflisch, B. I. Cohen, A. M. Dimits, Particle simulation of coulomb collisions: Comparing the methods of takizuka & abe and nanbu, *J. Comp. Phys.* 227 (9) (2008) 4308–4329.
- [25] D. Veberic, Having fun with lambert w (x) function, arXiv preprint arXiv:1003.1628.
- [26] J. Taylor, *Introduction to error analysis, the study of uncertainties in physical measurements*, 1997.
- [27] D. R. Welch, D. V. Rose, R. E. Clark, T. C. Genoni, T. Hughes, Implementation of an non-iterative implicit electromagnetic field solver for dense plasma simulation, *Computer physics communications* 164 (1) (2004) 183–188.
- [28] D. H. Munro, Interpreting inertial fusion neutron spectra, *Nuclear Fusion* 56 (3) (2016) 036001.
- [29] B. Appelbe, J. Chittenden, The production spectrum in fusion plasmas, *Plasma Physics and Controlled Fusion* 53 (4) (2011) 045002.